Mechanical and Chemical Spinodal Instabilities in Finite Quantum Systems

M. Colonna,[1] Ph. Chomaz,[2] and S. Ayik[3]
[1]*Laboratori Nazionali del Sud, Via S. Sofia 44, I-95123 Catania, Italy*
[2]*GANIL (DSM-CEA/IN2P3-CNRS), B.P. 5027, F-14021 Caen cedex, France*
[3]*Tennessee Technological University, Cookeville, Tennessee 38505*
(Received 30 October 2001; published 6 March 2002)

Self-consistent quantum approaches are used to study the instabilities of finite nuclear systems. The frequencies of multipole density fluctuations are determined as a function of dilution and temperature for several isotopes. The spinodal region of the phase diagrams is determined, and it appears that instabilities are reduced by finite size effects. The role of surface and volume instabilities is discussed. It is indicated that the important chemical effects associated with mechanical disruption may lead to isospin fractionation.

DOI: 10.1103/PhysRevLett.88.122701 PACS numbers: 25.70.Pq, 21.60.Ev, 21.60.Jz, 21.65.+f

The dynamics of first order phase transitions is often induced by instabilities against fluctuations of the order parameter. For instance, mechanical instabilities lead to liquid-gas phase transitions and chemical instabilities induce spinodal decomposition of binary alloys. In violent heavy ion collisions, nuclear matter may be pushed inside the coexistence region of the nuclear liquid-gas phase diagram. Then, the observed abundant fragment formation may take place through a rapid amplification of spinodal instabilities. New experimental results pleading in favor of such a spinodal decomposition have recently been reported [1,2]. From the theoretical point of view, the spinodal instabilities in finite systems have been mainly studied within a semiclassical or hydrodynamical framework [3–7]. However, since the relevant temperatures are comparable to the shell spacing and the wave numbers of the unstable modes are of the order of Fermi momentum, quantum effects are expected to be important, as stressed in [8,9].

In this Letter, we present a fully quantal investigation of the spinodal instabilities and related phase diagrams of finite nuclear systems. We determine frequencies and form factors of the unstable collective modes of an excited expanded system by linearizing the time-dependent Hartree Fock (TDHF) equation. We carry out applications for Ca and Sn isotopes. The quantum nature of the system is responsible for many dominant features such as the fact that the first mode to become unstable is the low lying octupole vibration. Slightly diluted systems are unstable against low multipole deformations of the surface, which may be associated with asymmetric binary or ternary fission processes. We extend our analysis to charge asymmetric systems and show the importance of chemical effects in the spinodal fragmentation process.

In TDHF theory, the evolution of the one-body density matrix $\tilde{\rho}(t)$ is determined by $i\hbar\partial_t\tilde{\rho}(t) = [h[\tilde{\rho}], \tilde{\rho}(t)]$, where $h[\tilde{\rho}] = \mathbf{p}^2/2m + U[\tilde{\rho}]$ is the mean-field Hamiltonian with $U[\tilde{\rho}]$ as the self-consistent potential. To investigate instabilities encountered during the evolution of an expanding system, one should study the dynamics of the small deviations $\delta\tilde{\rho}(t)$ around the TDHF trajectory $\tilde{\rho}(t)$ [10]. It is more convenient to carry out such an investigation in the "comoving frame" of the system, which is described by the density matrix, $\rho(t) = U^\dagger(t)\tilde{\rho}(t)U(t)$ where $U(t) = \exp[-\frac{i}{\hbar}\lambda t Q]$ with Q as a one-body operator. For example, in our case Q could be a suitable constraining operator for preparing the system at low densities and λ is the associated Lagrange multiplier. Then, the TDHF equation in the moving frame transforms into

$$i\hbar\frac{\partial}{\partial t}\rho(t) = [h(t) - \lambda Q, \rho(t)], \tag{1}$$

where the mean-field Hamiltonian in the moving frame is given by $h(t) = U^\dagger(t)h[\tilde{\rho}]U(t)$. The small density fluctuations $\delta\rho(t)$ in the moving frame are determined by the time-dependent RPA equations,

$$i\hbar\frac{\partial}{\partial t}\delta\rho = [h(t) - \lambda Q, \delta\rho] + [\delta U, \rho]. \tag{2}$$

Here we consider the early evolution of instabilities in the vicinity of an initial state ρ_0 determined by a constrained Hartree-Fock solution $[h(0) - \lambda Q, \rho_0] = 0$, where $h(0) = h[\rho_0] \equiv h_0$ is the mean-field Hamiltonian at the initial state. Then, small density fluctuations are characterized by the RPA modes ρ_ν and the associated frequencies ω_ν. Incorporating the representation $|i\rangle$, which diagonalizes $h_0 - \lambda Q$ and ρ_0 with eigenvalues ϵ_i and occupation numbers n_i, the equations for the RPA functions $\langle i|\rho_\nu|j\rangle = \rho_\nu^{ij}$ become

$$\hbar\omega_\nu\rho_\nu^{ij} = (\epsilon_i - \epsilon_j)\rho_\nu^{ij} + \sum_{kl}(n_j - n_i)V_{il,kj}\rho_\nu^{kl}, \tag{3}$$

where $V_{il,kj} = \langle i|\partial U/\partial\rho_{lk}|j\rangle$ denotes the residual interaction [10,11]. When the frequency of a mode drops to zero and then becomes imaginary, the system enters an instability region.

To perform an extensive study of instabilities we may parametrize the possible densities ρ_0 either by static Hartree-Fock (HF) calculations constrained by a set of

collective operators [12] or by using a direct parametrization of the density matrix. We follow the second approach by introducing a self-similar scaling of the HF density as suggested by dynamical simulations.

We solve the HF equation for the ground state $[h_{\mathrm{HF}}, \rho_{\mathrm{HF}}] = 0$, leading to the single-particle wave functions $|\varphi_i\rangle$ and the associated energies ε_i. We introduce the density matrix at a finite temperature T as $\rho_{\mathrm{HF}}[T] = 1/\{1 + \exp[(h_{\mathrm{HF}} - \varepsilon_F[T])/T]\}$, where $\varepsilon_F[T]$ is the corresponding Fermi level that is tuned in order to get the correct particle number. We perform a scaling transformation, $R[\alpha]$, which inflates the wave functions in radial direction by a factor α according to $\langle r|R[\alpha]|\varphi\rangle = \alpha^{-1/3}\langle r/\alpha|\varphi\rangle$. We define the density matrix for a hot and diluted system by $\rho_0[\alpha, T] = R[\alpha]\rho_{\mathrm{HF}}[\alpha^2 T]R^\dagger[\alpha]$. The associated constrained Hamiltonian is thus $\bar{h}_0[\alpha] = \alpha^2 R[\alpha]h_{\mathrm{HF}}R^\dagger[\alpha]$ so that the constraint can be identified as $-\lambda Q_\alpha = \bar{h}_0[\alpha] - h[\rho_0[\alpha, T]]$. By construction $[\bar{h}_0[\alpha], \rho_0[\alpha, T]] = 0$, so that they can be diagonalized simultaneously. The eigenstates of the constrained Hamiltonian are given by $|i\rangle = R[\alpha]|\varphi_i\rangle$, and the corresponding energies and occupation numbers are $\epsilon_i = \varepsilon_i/\alpha^2$ and $n_i = 1/\{1 + \exp[(\varepsilon_i - \varepsilon_F[\alpha^2 T])/\alpha^2 T]\}$, respectively.

We perform the HF calculations in the coordinate representation using the Skyrme force SLy4 [13]. We note that the isospin symmetry is already broken at the HF level. The particle and hole states are obtained by diagonalizing the HF Hamiltonian in a large harmonic oscillator representation [14], which includes 12 major shells for Ca isotopes and 15 for Sn. We apply the scaling and heating procedures described above to the density matrix, and calculate the residual interaction in a self-consistent manner. We solve the RPA Eq. (3) by a direct diagonalization using a discrete two quasiparticle excitation representation [15].

The top part of Fig. 1 shows calculations performed for ^{40}Ca. Top panels show contour plots of the isoscalar strength function associated with the isoscalar operator $A^s_{LM} = \sum_{i=1}^{A} r_i^L Y_{LM}$, with multipolarity $L = 2$–5, as a function of the dilution parameter α. In the stable domain, the energy associated with the dominant isoscalar strength decreases as dilution becomes larger, and at a critical dilution it drops to zero. At larger dilution, the system becomes unstable, and for each multipolarity, one or two unstable modes appear. This is illustrated in the bottom panel, where the "energy" of the mode $E_\nu = -i\hbar\omega_\nu$ is plotted as a function of the dilution.

It is seen that at low dilutions, around $\alpha = 1.2$, only the octupole mode becomes unstable. In general, density fluctuations with odd multipolarity become unstable at relatively smaller values of dilution than those for even multipole fluctuations. This is a genuine quantum effect, due to the fact that the majority of the particles have to jump only one major shell to produce an odd natural-parity particle-hole excitation while twice this energy is required for an even one. In nuclei at normal density this makes the first 3^- a strongly collective low lying state;

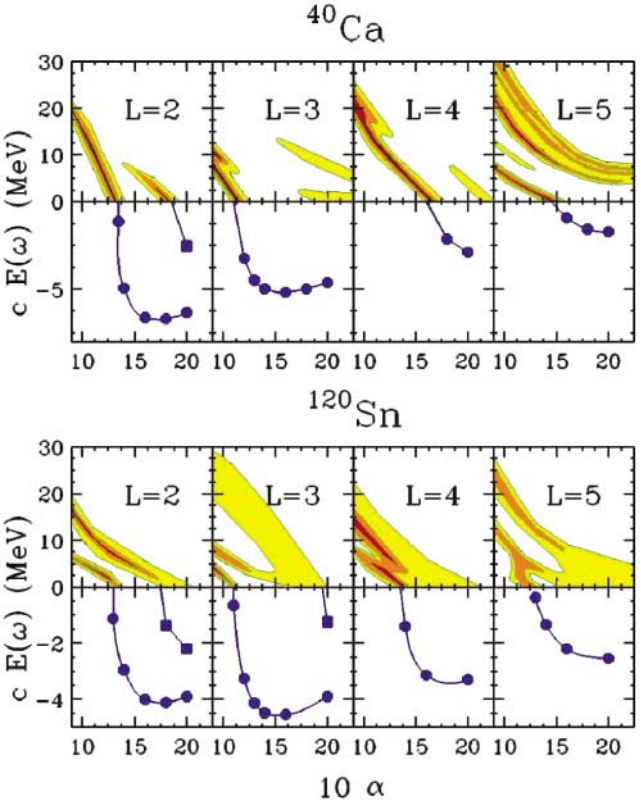

FIG. 1 (color). Contour plots of the isoscalar strength functions associated with the multipolarity $L = 2$–5 as a function of the dilution parameter α and the collective energy of the mode $E_\nu = c\hbar\omega_\nu$ ($c = 1$ for stable modes, $-i$ for unstable modes) for ^{40}Ca (top) and ^{120}Sn (bottom). The strength values are given in percentage of the EWSR: 2 (yellow), 15 (orange), and 30 (red).

in a diluted system this state is the first to turn unstable. The second feature is that large multipole deformations are hardly becoming unstable. This is due to surface and quantum effects that prevent the breakup of such a small system into several fragments. As a consequence, the fastest growth time, $\tau_\nu = \hbar/|E_\nu| \approx 28$ fm/c, occurs for $L = 2$ at the dilution $\alpha = 1.8$. However, deep inside the instability region, the octupole mode is almost as unstable as the quadrupole mode.

Results of similar calculations performed for ^{120}Sn are shown in the bottom part of Fig. 1. Also in this case, the octupole mode becomes unstable first, at $\alpha \approx 1.1$. Large multipoles are more unstable in ^{120}Sn than in ^{40}Ca, since the system is larger and can afford larger multipole deformations. This is the reason why the smallest growth time in ^{120}Sn occurs for $L = 3$.

It is useful to study the behavior of the RPA solution in the coordinate space, $\rho^+_{p,n}(\mathbf{r}) \equiv \rho^+_{p,n}(\mathbf{r}, \mathbf{r})$, for protons and for neutrons separately. Since the unstable modes have large isoscalar strength, protons and neutrons mostly move in phase. However, because of the isospin symmetry breaking induced by the Coulomb force and by the initial asymmetry of the system considered, neutrons' and

protons' oscillations have different amplitude and shape. Figure 2(a) shows the radial dependence of the form factor associated with the unstable octupole mode, at the dilution $\alpha = 1.5$, for protons (dotted line), neutrons (full line), and the sum (dashed line), in Sn isotopes. Contour plots of neutron (proton) perturbed densities, $\rho_{0p,n}(\mathbf{r}) + \rho^{+}_{p,n}(\mathbf{r})$, are also shown in Figs. 2(b) and 2(c).

We observe that proton oscillations are mostly located at the surface of the system, which is a way to minimize the Coulomb repulsion energy. At the same time neutrons try to follow protons; however, this motion is strongly affected by the isospin initial asymmetry and the difference between the neutron and proton orbitals at the Fermi energy. In fact, in neutron-rich systems, much larger proton oscillations are observed, that is, a way to form more symmetric fragments and hence to reduce the symmetry energy. The last effect is particularly evident in the neutron-rich ^{132}Sn for which the neutrons are more difficult to put in motion. We observe a quite complex structure of the unstable modes: Volume and surface instabilities are generally coupled and cannot be easily disentangled, as well as isoscalar and isovector excitations, since protons and neutrons do not move in the same way. Figure 3 shows the correlations between the amplitude of proton fluctuations $\rho^{+}_{p}(r)$ and neutron fluctuations $\rho^{+}_{n}(r)$, obtained at a radial distance r ranging from 0 to the system radius R, for the octupole mode. The different panels correspond to the three Sn isotopes considered and to three dilutions, α, indicated in the figure. The correlations describe closed paths, since $\rho^{+}_{p,n}(r)$ starts from zero at $r = 0$ and goes to zero again at large distances.

When protons and neutrons fluctuate without changing the local chemical ratio, one should have $\rho^{+}_{p}(r) = \rho^{+}_{n}(r)Z/N$ (full line). An identical motion of the two fluids should follow the diagonal $\rho^{+}_{p}(r) = \rho^{+}_{n}(r)$ (dashed line). In $N = Z$ nuclei [Fig. 3(a)] the motion of protons and neutrons should be the same (isoscalar excitations); however, the Coulomb force introduces small differences. As seen in Fig. 2, in diluted systems ($\alpha > 1$), we observe that, in the vicinity of the nuclear surface, density fluctuations are larger for protons than for neutrons, especially in the case of neutron-rich unstable isotopes, ^{120}Sn and ^{132}Sn [see Figs. 3(b) and 3(c)], leading to a reduction of the asymmetry of the fragments produced at the surface. In the interior we observe, for these isotopes, an interesting evolution from $\rho^{+}_{p}(r) < \rho^{+}_{n}(r)Z/N$ for $\alpha = 1$ (stable modes) to $\rho^{+}_{p}(r) > \rho^{+}_{n}(r)Z/N$ for the dilute systems. Hence we observe a change of the local chemical ratio, leading to a reduction of the symmetry energy, also in the interior of the system. This effect may be related to the isospin fractionation that occurs in unstable asymmetric nuclear matter [16]. The proton migration towards the large density domains is more frequent than the neutron migration, which may lead to formation of more symmetric fragments.

We also carry out calculations at finite temperature and determine the dilutions at which different unstable modes begin to appear. This allows us to specify the border of

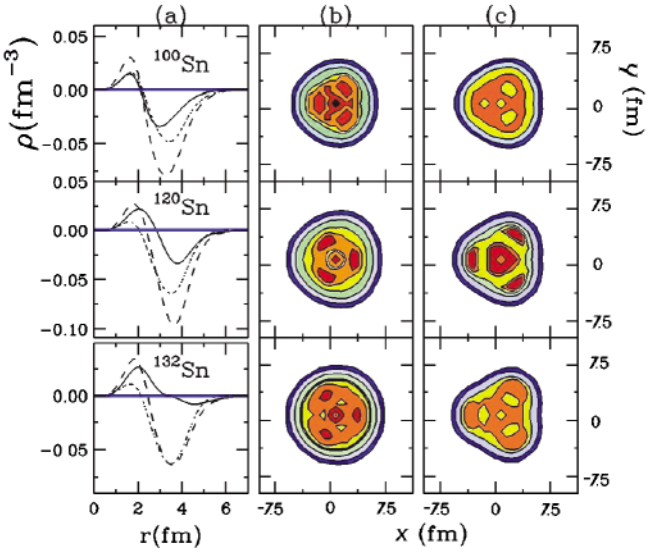

FIG. 2 (color). (a) Radial dependence of the form factor associated with the unstable mode with $L = 3$, at the dilution $\alpha = 1.5$, for protons (dotted line), neutrons (full line), and the sum (dashed line). The radial distance is scaled by the dilution parameter α. (b) Contour plots of the neutron perturbed density. From the surface to the center, the contour lines correspond to the density values: 0.0037, 0.0075, 0.015, and 0.023 fm^{-3}. For larger density, colors show small density variations (3%). (c) Same for protons.

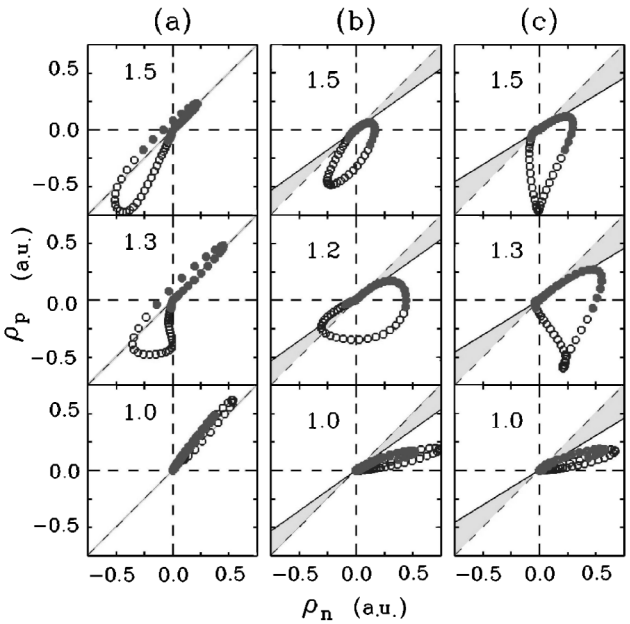

FIG. 3. Correlations between the amplitude of proton and neutron fluctuations, for several dilutions. The full circles correspond to a radial distance $0 < r < 2.4\alpha$ fm, and the open circles correspond to 2.4α fm $< r < R$. The dashed line indicates $\rho^{+}_{p} = \rho^{+}_{n}$, the full line corresponds to $\rho^{+}_{p} = \rho^{+}_{n}Z/N$. Results are shown for ^{100}Sn (a), ^{120}Sn (b), and ^{132}Sn (c).

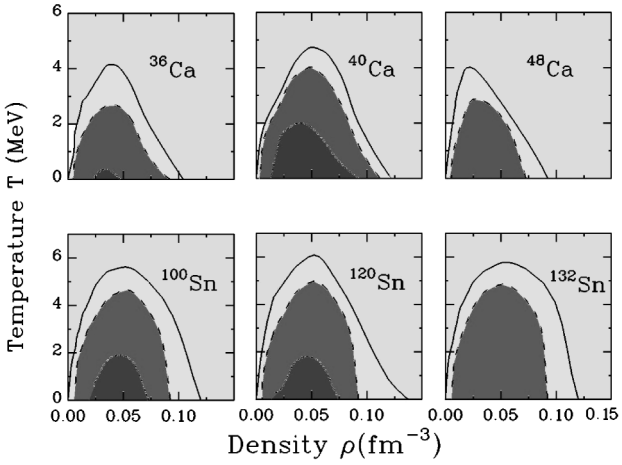

FIG. 4. Border of the instability region (full line) associated with $L = 3$, for Ca and Sn isotopes. The dashed line connects the points having the instability growth time $\tau = 100$ fm/c. The dots are associated with $\tau = 50$ fm/c.

the instability region in the density-temperature plane for different unstable modes. Figure 4 shows phase diagrams for octupole instabilities in Sn and Ca isotopes.

Here, for simplicity, we define the density as $\rho = \rho_0/\alpha^3$. The full line indicates the border of the instability region. The dashed line connects points that are associated with the instability growth time $\tau = 100$ fm/c, and the dots correspond to situations (if any) with a shorter growth time $\tau = 50$ fm/c. The instability region appears quite reduced as compared to that of nuclear matter. The limiting temperature for instability to occur is around 6 MeV for Sn and 4.5 MeV for Ca while it is about 16 MeV in symmetric nuclear matter. Heavier systems have a larger instability region than the lighter ones. Moreover, more asymmetric systems are less unstable. In fact, in spite of the larger mass, ^{132}Sn is less unstable than ^{120}Sn. Larger instability growth times are obtained for ^{132}Sn. As seen from phase diagrams for ^{36}Ca and ^{40}Ca, the region of instability is reduced also in proton-rich systems. This behavior is in agreement with nuclear matter calculations, which indicates that the instability region shrinks in asymmetric nuclear matter [16].

In conclusion, we have presented a study of the early development of spinodal instabilities in finite nuclear systems by employing a quantal RPA approach. Results are relevant for multifragmentation studies; in fact, dominant unstable modes determine the onset of the subsequent fragmentation of the system that has to be followed using a full dynamical calculation. We have investigated isospin effects on instabilities by carrying out calculations for Ca and Sn isotopes. We find that instabilities are mostly of isoscalar nature, but contain also an important isovector component in asymmetric matter. Hence the liquid-gas separation of asymmetric systems is always linked to a chemical separation inducing a fractional distillation of the system. The degree of instability in neutron-rich and also proton-rich nuclei appears reduced as compared to that of symmetric nuclei of comparable size. The instabilities are also reduced in small nuclei. Finally we have stressed important quantum effects, such as the octupolar nature of the most important instability.

The authors acknowledge the Yukawa Institute for Theoretical Physics, S. A. and M. C. acknowledge GANIL, and Ph. C. acknowledges LNS, where parts of this work have been carried out, for support and warm hospitality. Stimulating discussions with M. Di Toro and D. Lacroix are also acknowledged. This work is supported in part by the U.S. DOE Grant No. DE-FG05-89ER40530.

[1] L. Beaulieau *et al.,* Phys. Rev. Lett. **84**, 5971 (2000).
[2] B. Borderie *et al.,* Phys. Rev. Lett. **86**, 3252 (2001).
[3] G. F. Bertsch and P. J. Siemens, Phys. Lett. **126B**, 9 (1983).
[4] H. Heiselberg, C. J. Pethick, and D. G. Ravenhall, Phys. Rev. Lett. **61**, 818 (1988).
[5] W. Nörenberg, G. Papp, and P. Rozmej, Eur. Phys. J. A **9**, 327 (2000).
[6] M. Colonna, Ph. Chomaz, and J. Randrup, Nucl. Phys. **A567**, 637 (1994); A. Guarnera, M. Colonna, and Ph. Chomaz, Phys. Lett. B **373**, 267 (1996).
[7] B. Jacquot, S. Ayik, Ph. Chomaz, and M. Colonna, Phys. Lett. B **383**, 247 (1996).
[8] S. Ayik, M. Colonna, and Ph. Chomaz, Phys. Lett. B **353**, 417 (1995).
[9] B. Jacquot, M. Colonna, S. Ayik, and Ph. Chomaz, Nucl. Phys. **A617**, 356 (1997).
[10] D. Vautherin and M. Veneroni, in *Microscopic Approaches to Nuclear Structure Calculations, Proceedings of the First International Spring Seminar on Nuclear Physics, Sorrento, Italy, 1986* (Italian Physical Society, Bologna, Italy, 1986).
[11] P. Ring and P. Shuck, *The Nuclear Many-Body Problem* (Springer-Verlag, New York, 1980).
[12] H. Sagawa and G. F. Bertsch, Phys. Lett. **146B**, 138 (1984); **155B**, 11 (1985).
[13] E. Chabanat *et al.,* Nucl. Phys. **A627**, 710 (1997); **A635**, 231 (1997); **A643**, 441(E) (1998).
[14] N. Van Giai and H. Sagawa, Nucl. Phys. **A371**, 1 (1981).
[15] D. Vautherin and N. Vinh Mau, Nucl. Phys. **A422**, 140 (1984).
[16] Bao-An Li and C. M. Ko, Nucl. Phys. **A618**, 498 (1997); V. Baran, M. Colonna, M. Di Toro, and V. Greco, Phys. Rev. Lett. **86**, 4492 (2001).